## ANALYSIS

Check for updates

# Supply risk considerations for photoelectrochemical water splitting materials†

Martin Hillenbrand, [ID] [a] Christoph Helbig [ID] *[a] and Roland Marschall [ID] [b]

Hydrogen is a key enabler of a carbon neutral economy. The main production route of renewable hydrogen is *via* renewable wind and solar power and water splitting *via* electrolyzers. Photo-electrochemical water splitting is an alternative production route using incoming solar radiation to produce hydrogen and oxygen *via* a photoabsorber material with suitable band gaps and positions. Various absorber materials are being discussed in research and further developed at the lab scale. However, these materials need to be scalable in production, with low supply risk, because of the scale of hydrogen production needed to satisfy the global need for green hydrogen. Here, we semi-quantitatively assess the short-term and long-term supply risks due to potential supply reduction, demand increase, concentration risks, and political risks of eight chemical elements contained in nine promising absorber materials for photoelectrochemical water splitting. On an element level, supply risks are lowest for iron, copper, and tantalum in the present scenario and tin in the future scenario. The supply risks are highest for bismuth in the present scenario and future scenario. On a material level, present supply risks are lowest for hematite and highest for bismuth vanadate. Bismuth vanadate has the highest future supply risks, but tin tungsten oxide achieves the lowest supply risk score in the future scenario. The results show that some frequently discussed photoelectrochemical absorber materials have higher supply risks than typically perceived. In contrast, other materials should be more intensively studied because of their promising low long-term supply risk evaluation. Our method provides a separate assessment of present and future supply risks, which was previously unavailable for the criticality assessments.

**Broader context**

Photoelectrochemical water splitting is a technology to directly generate hydrogen and oxygen from water using sunlight. It is an alternative to the two-stage process of photovoltaics and electrolysis. For a widespread use of photoelectrochemistry, absorber materials are required that have good electrochemical properties and are simultaneously abundant with low supply risks. In this article, we systematically quantify the supply risks of good photoabsorbers to identify those which are most promising for large-scale hydrogen production globally.

## Introduction

Hydrogen is a potentially clean energy carrier that can store solar energy, central to a net-zero carbon emissions energy system.[1] Hydrogen is also in demand as a chemical, for steel production, or for fertilizer feedstock. Currently, most hydrogen is produced as grey hydrogen, a by-product of petrochemical plants.[2]

In the future, green hydrogen, produced from renewable energy sources without emitting greenhouse gases, will be needed in much larger quantities.[3] For now, production capacity is limited, partly due to a lack of renewable electricity generation at sufficiently low cost, and technology development is needed to scale up production and reduce the costs of green hydrogen.[4] To compete with grey hydrogen, green hydrogen production costs would likely have to get below 2 USD per kg.[5]

To date, most efforts have been made to improve the production route of green hydrogen through a combination of photovoltaics or wind power and electrolysis. This two-step process is expensive and requires using critical raw materials (CRMs) like platinum group metals and rare earth elements.[6] CRMs are materials of concern because of their multi-faceted

[a] *Ecological Resource Technology, University of Bayreuth, Universitätsstr. 30, 95447 Bayreuth, Germany. E-mail: christoph.helbig@uni-bayreuth.de*
[b] *Physical Chemistry III, University of Bayreuth, Universitätsstr. 30, 95447 Bayreuth, Germany*

This journal is © The Royal Society of Chemistry 2024

*Energy Environ. Sci.,* 2024, **17**, 2369–2380 | **2369**

supply risks and potential vulnerabilities to supply restrictions on global, national, or company levels.[7,8] Any energy technology used at large-scale will have to consider the abundance and the supply of the elements contained within.[9] Alternatively, one-step hydrogen generation with solar light is possible *via* photocatalytic (PC) or photoelectrochemical (PEC) water splitting.[10] Both PC and PEC activate the water splitting redox reaction by photo-absorption rather than by applying an external voltage in electrolysis.

Further, photoelectrochemical water splitting has an advantage over photocatalytic water splitting because the hydrogen and oxygen created are automatically physically separated at the anode and cathode of the photoelectrochemical cell. Therefore, hydrogen can be collected at one side, and back reaction of the two gases can easily be avoided. Moreover, water splitting photocatalyst panel reactors have already been built as demonstrators.[11]

The redox reaction of water splitting requires an energy of 1.23 eV, but the practical limit for an optimal material is around 2 eV due to the overpotentials required. This energy level corresponds to a wavelength of 610 nm.[12] Semiconductors with smaller band gaps or unsuitable band positions for overall water splitting can be used in tandem cells,[13] which will be discussed later. If the band gap is larger than the required 2 eV, a lower share of the incoming solar radiation is utilized for the water splitting reaction. Therefore, ideal materials for photoelectrochemical water splitting have band gaps slightly above 2 eV, corresponding to a theoretical solar-to-hydrogen (STH) efficiency of about 20%. Correcting the theoretical STH in PEC is necessary if a bias is applied to move the band potential upwards towards 0 V *versus* the reference hydrogen electrode.[14]

The advantages of photoelectrochemical water splitting over the two-stage process of photovoltaics and electrolysis are higher intrinsic acceptance of the day-night cycle (electrolysis should be running continuously to avoid rapid aging of its components), efficient use of incoming thermal radiation for improved reaction kinetics, and less CRM reliance. Disadvantages of photoelectrochemical water splitting are a lack of long-term stability because of photo-corrosion of some photocatalysts and the criticality of some coating and fabrication processes.[15] In a cost comparison, the PEC and photovoltaics combined with electrolysis reached similar levels in the past, with a strong dependence on the price of electricity and the hydrogen generation efficiency.[16]

In this article, we estimate the supply risks of large-scale PEC water splitting with a range of promising absorber materials. In the past, only a few materials supply risk assessments have been conducted for renewable energy technologies, including PEC water splitting, which have also not reported clear statements on current and future supply risks.[9] We apply supply risk estimations using various indicators from raw material criticality assessment methods.[17] We have chosen the most representative oxide absorber materials in literature from the last decade to discuss the criticality and sustainability of the most efficient and most investigated materials. We find that on a material level, present supply risks are lowest for

tantalum nitride and highest for bismuth vanadate. Bismuth vanadate has the highest future supply risks, but tin tungsten oxide achieves the lowest supply risk score in the future scenario. The results show that some frequently discussed photoelectrochemical absorber materials have higher supply risks than typically perceived.

## Materials

Photoelectrochemistry (PEC) is based on generating charge carriers in a semiconductor upon light irradiation,[18] supposing the energy of the incident photons is larger than the band gap of the used semiconductor. In that case, electron–hole-pairs are generated in the semiconductor,[19] the latter being processed as a photoelectrode thin film. In the case of PEC water splitting, one of the photogenerated charge carriers is used to reduce or oxidize water, and the other charge carrier is transported along an external electrical circuit to the counter electrode.[20] If the semiconductor electrode oxidizes water as a photoanode, the photogenerated electrons will reduce protons to hydrogen at the counter electrode, *e.g.*, a platinum wire. A typical lab-scale setup for such a one-compartment cell is shown in Fig. 1, including the photoelectrode clamped onto the cell body of a so-called cappuccino-type cell. Such a cappuccino cell allows both front- and back-side illumination. An industrial-scale setup is still under development.[21,22]

Ultimately, the amount of hydrogen produced is connected to the amount of photogenerated electrons upon light irradiation that can be transported to the counter electrode.[14] Thus, utilizing the AM1.5G standardized solar spectrum, a high number of absorbed photons is of utmost importance since each photon absorbed generates one photoelectron (but due to recombination, not every photogenerated electron will reach the counter electrode). The band gap of the semiconductor determines the number of photons absorbed.

The band gap of a semiconductor is the energy difference between the valence band and the conduction band. Since both bands are formed from the linear combination of the atomic orbitals of the used elements, the band gap and band positions of a semiconductor are directly connected to the elements used and the crystal structure formed. Choosing the right elements to form the absorber semiconductor can thus tailor the amount of photogenerated charge carriers, immediately leading to the question of the restrictions for the elements of choice, with a scalable application for water splitting in mind.

Should the use of scarce and critical elements to generate photoelectrodes with small band gaps be justified by the purpose of generating green hydrogen? Regarding the need for an energy transition, the scalability of PEC water splitting is of utmost importance, and cheap preparation techniques will also be necessary.[23] On the other hand, higher efficiencies could justify the use of more expensive and scarce elements. The absorption coefficient of a semiconductor might also lead to using more of the material to generate films thick enough to absorb all incident light.
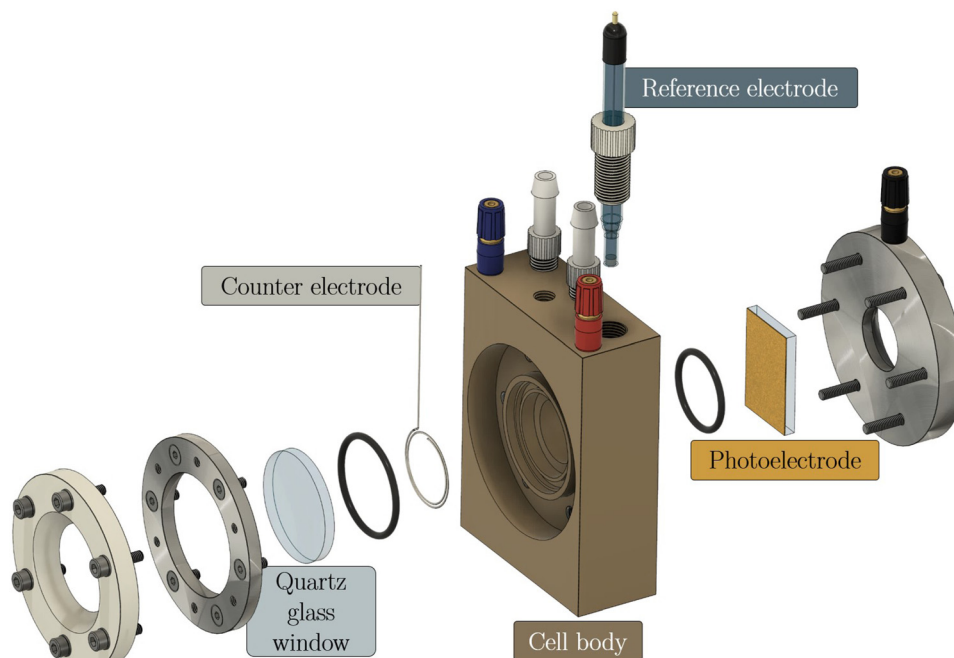
**2370** | *Energy Environ. Sci.*, 2024, **17**, 2369–2380

This journal is © The Royal Society of Chemistry 2024

**Fig. 1** A typical lab-scale PEC cell by Zahner with one compartment, with the photoelectrode pressed against an o-ring of the compartment (cappuccino-type cell).

A sustainable choice of elements for PEC water splitting is often discussed in the community.[24,25] It is generally accepted that cheap and stable materials are needed for photoelectrodes. Likewise, cheap preparation techniques are needed to process the materials into viable photoelectrodes. However, a quantitative analysis has not yet been performed. Therefore, we have chosen the most representative oxide absorber materials in literature from the last decade to discuss the criticality and sustainability of the most efficient and most investigated materials. We have excluded sulfide materials due to their lack of stability, and we have excluded III–V (multilayer) photoelectrodes here despite showing very high efficiencies because they are known to require very expensive processing.[26]

In PEC, if the band positions of the used semiconductor do not straddle the water splitting potentials, a supporting bias can be applied to drive one photogenerated charge carrier to the counter electrode. Tandem photoelectrodes have been developed to overcome this energy input while extending light absorption and widening the electrochemical window.[20] Alternatively, combinations with photovoltaic (PV) materials like silicon have been developed,[27] again for multiphoton absorption and improved charge carrier separation. Some of our chosen materials (see Table 1) can be used to form good PEC-PV combinations with buried junctions, but we have not chosen the discussed materials for tandem devices yet. Tandem cells can be considered in a future assessment.

Harsh electrolyte environments in PEC water splitting can lead to the corrosion of photoelectrodes. Thus, surface layers are often needed to protect the absorber from the electrolyte contact while still being transparent for the charge carrier transfer to the electrolyte. Moreover, electrocatalysts on the absorber/protection layer are needed to improve the kinetics of charge carrier transfer to the electrolyte, especially for the water oxidation half-reaction. Since the current densities in PEC are much lower than in electrochemical water splitting, noble metals can be more easily substituted.

**Table 1** Most discussed absorber materials for photoelectrochemical water splitting and their key properties

| Absorber material (formula) | Absorber material (name) | Band gap/eV | Theoretical max photocurrent under AM1.5G/mA cm$^{-2}$ | Theoretical STH | Highest reported photocurrent under AM1.5G/mA cm$^{-2}$ | Typical protection material[28] | Material-specific references |
|---|---|---|---|---|---|---|---|
| CuO | Cupric oxide | 1.4 | −35 | 43% | −6.3@0.0 V vs. RHE | TiO$_2$ | 29 and 30 |
| Cu$_2$O | Cuprous oxide | 2.0 | −14.7 | 18% | −10@0.0 V vs. RHE | TiO$_2$, SnO$_2$, AZO | 31–33 |
| CuBi$_2$O$_4$ | Copper bismuth oxide | 1.5–1.8 | Up to −29.0 | 24–35% | −1.0@0.0 V vs. RHE | TiO$_2$, CdS/TiO$_2$ | 34–36 |
| BiVO$_4$ | Bismuth vanadate | 2.4 | 7.5 | 9.2% | 6.7@1.23 V vs. RHE | FeOOH/NiOOH, CoO$_x$ | 31 and 37 |
| Ta$_3$N$_5$ | Tantalum nitride | 2.1 | 12.9 | 15.9% | 12.1@1.23 V vs. RHE | TiO$_x$, FeNiCoO$_x$ | 38 |
| α-Fe$_2$O$_3$ | Hematite | 2.2 | 10.5 | 12.9% | 4.6@1.23 V vs. RHE | NiFeO$_x$, IrO$_x$ | 31, 39 and 40 |
| ZnFe$_2$O$_4$ | Zinc ferrite | 2.2 | 10.5 | 12.9% | 1.0@1.23 V vs. RHE | Al$_2$O$_3$ | 41–43 |
| WO$_3$ | Tungsten trioxide | 2.7 | 4.8 | 5.9% | 3.7@1.23 V vs. RHE | —, FeOOH | 31, 37 and 44 |
| α-SnWO$_4$ | Tin tungsten oxide | 1.9 | 17 | 20.9% | 1.05@1.23 V vs. RHE | NiO | 45–47 |

This journal is © The Royal Society of Chemistry 2024

*Energy Environ. Sci.*, 2024, **17**, 2369–2380 | **2371**

The chosen absorber materials here are amongst the most investigated in literature, namely cupric oxide (CuO), cuprous oxide ($Cu_2O$), copper bismuth oxide ($CuBi_2O_4$), bismuth vanadate ($BiVO_4$), tantalum nitride ($Ta_3N_5$), hematite ($\alpha$-$Fe_2O_3$), zinc spinel ferrite ($ZnFe_2O_4$), tungsten trioxide ($WO_3$), and tin tungsten oxide ($\alpha$-$SnWO_4$). Bismuth vanadate has the highest reported solar-to-hydrogen (STH) ratio of 8%.[37] Tantalum nitride has reached an STH of 4.07%.[48]

Typical protection materials are specific to the corresponding absorber materials and include iron(III) oxide-hydroxide, nickel(III) oxide-hydroxide, iridium oxide, titanium oxide, tin oxide, aluminum-doped zinc oxide (AZO), cobalt oxide, aluminum oxide, and cobalt(II,III) oxide. We know the need for these protection materials and their processing costs. Still, due to their minimal material requirements (often only applied through atomic layer deposition), their contribution to the supply risk is minimal. The same applies to the added co-catalysts with, for example, iridium oxide or cobalt oxide on the oxygen side and platinum group metals on the hydrogen side.

## Methods

The evaluation of supply risks in this article follows the approach for supply risk assessment on the technology level previously developed by some of the authors, also labelled as the "Augsburg method" for supply risk assessment.[7] This method has so far been applied to thin-film photovoltaics,[49] lithium-ion batteries,[50] and Ni-based superalloys.[51] The method evaluates semi-quantitatively the supply risk of metals and semi-metals in the technology on an element level. Here, this assessment is applied to the metal elements in the absorber material only: tungsten, iron, copper, bismuth, zinc, tin, tantalum, and vanadium. Oxygen and nitrogen components of the absorber materials are excluded from the assessment as they do not pose a supply risk.

The method contains four categories of indicators considered to estimate the relative supply risk for the elements: risk of supply reduction (S), risk of demand increase (D), market concentration (C), and political risk (P). Each category contains two to four indicators. Each indicator is calculated and normalized afterward to a common scale of 0 (lowest supply risk) to 100 (highest supply risk). This normalization enables a comparison of relative supply risks associated with various absorber materials. Each category is weighted with 25% of the total score, and all indicators within one category are weighted equally.

Compared with previous case studies for supply risk assessments by the authors, the indicators are all rephrased so that a higher indicator value relates to higher supply risk. This wording is

**Table 2** Supply risk indicators used in the assessment, their category, ID (for figures and tables), dimension of measurement, perspective (present scenario, future scenario), and the normalization formula to a 0 to 100 score

| Category | ID | Indicator | Dimension | Calculation | Perspective |
|---|---|---|---|---|---|
| Supply reduction | S1 | Scarcity, based on reserves | Years | $S1 = 100 - 0.2T - 0.008T^2$ $T = \dfrac{\text{Reserves}}{\text{Annual production}}$ | Present |
| | S2 | Scarcity, based on resources | Years | $S2 = 100 - 0.1T - 0.002T^2$ $T = \dfrac{\text{Resources}}{\text{Annual production}}$ | Future |
| | S3 | Dependence on primary production | % | $S3 = 100(1 - \text{EoLRIR})$ | Present + future |
| Demand increase | D1 | Demand growth | % | Annual production growth from future technologies $D1 = 1000\,DG$ $DG = \left(1 + \dfrac{\text{FTD}_{2040} - \text{FTD}_{2018}}{\text{Production}_{2018}}\right)^{\frac{1}{\text{years}}} - 1$ | Present + future |
| | D2 | By-product dependence | % | $D2$ = Percentage of global production obtained as companion | Present + future |
| | D3 | Sector competition | Qualitative | $D3 = SCI$ | Present |
| | D4 | Lack of substitution options | Qualitative | $D4$ = Substitute performance | Present + future |
| Concentration | C1 | Country concentration, based on production | HHI | $C1 = c_1 \ln HHI - d_1$ $HHI = 10\,000\sum p_i^2$ | Present |
| | C2 | Country concentration, based on reserves | HHI | $C2 = c_1 \ln HHI - d_1$ $HHI = 10\,000\sum \text{reserves}_i^2$ | Future |
| Political | P1 | Political instability (WGI-PV) | Qualitative | $P1 = 20\,(2.5 - WGI)$ $WGI = \sum \text{wgi}_i p_i$ | Present |
| | P2 | Regulation (PPI) | Qualitative | $P2 = (100 - PPI)$ $PPI = \sum \text{ppi}_i p_i$ | Present |
| | P3 | Regulation (HDI) | Qualitative | $P3 = 100 \cdot \dfrac{HDI - 0.352}{0.949 - 0.352}$ $HDI = \sum \text{hdi}_i p_i$ | Present |
| | P4 | Political instability (WGI-PV), based on reserves | Qualitative | $P4 = 20\,(2.5 - WGI)$ $WGI = \sum \text{wgi}_i\,\text{reserves}_i$ | Future |
| | P5 | Regulation (PPI), based on reserves | Qualitative | $P5 = (100 - PPI)$ $PPI = \sum \text{ppi}_i\,\text{reserves}_i$ | Future |
| | P6 | Regulation (HDI), based on reserves | Qualitative | $P6 = 100 \cdot \dfrac{HDI - 0.352}{0.949 - 0.352}$ $HDI = \sum \text{hdi}_i\,\text{reserves}_i$ | Future |

**2372** | *Energy Environ. Sci.*, 2024, **17**, 2369–2380

This journal is © The Royal Society of Chemistry 2024

in line with the list of most often used supply risk indicator categories identified by Helbig *et al.*[17] The fact that PEC is a future technology currently not produced on an industrial scale leads to the special question of how the supply risk assessment can be carried out in a future-looking perspective. The data sources for each supply risk indicator are typically one or several years old. They are only secondary data sources, with their primary data collection potentially reaching 5 to 10 years back into the past. Here, however, we are trying to assess the supply risks of a technology potentially widely used a decade into the future. Therefore, applying the indicators with a forward-looking variant is desirable, for which variants of individual indicators with a more future-oriented calculation have been implemented, or indicators have been assigned to either the present or the future scenario. Supply risk indicators differ between the present and the future scenarios, but the investigated indicator groups remain the same and are comparable within. Some indicators are used in both perspectives. Table 2 lists all indicators of the supply risk assessment, their supply risk category, measurement dimension, calculation, and allocation to present or future scenarios.

Some absorber materials contain multiple potentially critical elements. For these, aggregating the results for the individual elements to the absorber level is necessary. Multiple perspectives can be considered in this aggregation step. In the simple arithmetic mean approach, each contained element has the same weighting in the aggregation step. Mass-share and cost-share weighting approaches consider each element according to their contribution to the total weight of elements considered in the supply risk assessment or the total raw material costs. The maximum approach considers only the element with the highest supply risk score.

## Results

The supply risk assessment begins by determining the values for all 15 indicators for the present and future scenario for all

eight elements selected for this work. Table 3 lists all the key data for the indicators of supply risk assessment before normalization and their respective data sources.

The depletion time is interpreted as a scarcity indicator and is a measure of the market pressure for further exploration and mining expansion.[50] The volumes of production, reserves, and resources stem from the USGS Mineral Commodity Summaries. They are reported as mining production of the corresponding contained element, except for bismuth, which refers to the gross weight of refinery production.[52] For the present scenario, the depletion times of the eight elements range between 14 years for zinc and 244 years for vanadium. The low depletion time of reserves of 18 years for bismuth must be taken cautiously because the USGS has not reported new reserve information for bismuth since 2017.[53] Depletion times are calculated based on the resource volume range between 99 years for copper and multiple millennia for tungsten and tantalum.[52] End-of-life recycling input rates (EOL-RIR) are highest for tungsten at 42% and lowest for bismuth at 0%.[54,55] This indicator is used both in the present and future scenarios.

Significant demand growth from future technology demand is expected for tantalum, vanadium, and copper, with an additional annual demand growth emerging from future technologies of 3.1%, 2.5%, and 0.7%, respectively. In contrast, none of the future technologies considered by Marscheider-Weidemann *et al.* was estimated to rely on iron, zinc, tin, tungsten, or bismuth; therefore, 0% demand growth from future technologies was assumed.[56] Bismuth and vanadium are mainly produced as by-products.[57] 90% of bismuth are by-products of lead, tungsten, copper, tin, and molybdenum production, and 82% of vanadium is obtained during iron and aluminum extraction, the recovery from spent catalysts, that accumulated vanadium during the refinement of vanadium-containing crude oils, and uranium residues.[57] Tantalum is

**Table 3** Key data for the eight elements on an indicator level before normalization

| ID | Data | Unit | Vanadium | Iron | Copper | Zinc | Tin | Tantalum | Tungsten | Bismuth | Ref. |
|---|---|---|---|---|---|---|---|---|---|---|---|
| S1 | Depletion time, based on reserves | Years | 244 | 53 | 42 | 14 | 15 | 174 | 45 | 18 | 52 and 53 |
| S2 | Depletion time, based on resources | Years | 600 | 141 | 99 | 150 | 1510 | 34 768 | 4536 | 419 | 52 |
| S3 | End-of-life recycling input rate | % | 1 | 23 | 22 | 10 | 31 | 1 | 42 | 0 | 54 and 55 |
| D1 | Future technology demand | % | 2.5 | 0.0 | 0.7 | 0.0 | 0.0 | 3.1 | 0.0 | 0.0 | 56 |
| D2 | By-product ratio | % | 82 | 1 | 9 | 10 | 3 | 28 | 5 | 90 | 57 |
| D3 | Sector competition index | 0 to 100 | 13 | 24 | 36 | 17 | 49 | 57 | 36 | 31 | 55 and 58 |
| D4 | Substitution | 0 to 100 | 63 | 57 | 70 | 38 | 36 | 41 | 53 | 46 | 59 |
| C1 | HHI, based on production | HHI | 4952 | 1885 | 1278 | 1694 | 1740 | 2533 | 7232 | 6560 | 52 |
| C2 | HHI, based on reserves | HHI | 2789 | 1767 | 1334 | 1970 | 1229 | 4304 | 3782 | 4662 | 52 and 53 |
| P1 | World governance indicator (WGI), based on production | −2.5 to 2.5 | −0.53 | −0.03 | −0.21 | −0.18 | −0.66 | −0.99 | −0.42 | −0.25 | 52 and 60 |
| P2 | Policy perception indicator (PPI), based on production | 0 to 100 | 49 | 52 | 47 | 43 | 36 | 27 | 40 | 37 | 52 and 61 |
| P3 | Human development indicator, based on production | 0 to 1 | 0.77 | 0.82 | 0.68 | 0.67 | 0.71 | 0.57 | 0.75 | 0.76 | 52 and 62 |
| P4 | World governance indicator (WGI), based on reserves | −2.5 to 2.5 | −0.16 | −0.03 | −0.08 | 0.06 | −0.56 | −0.07 | −0.29 | −0.34 | 52, 53 and 60 |
| P5 | Policy perception indicator (PPI), based on reserves | 0 to 100 | 59 | 52 | 45 | 60 | 39 | 55 | 29 | 33 | 52, 53 and 61 |
| P6 | Human development indicator, based on reserves | 0 to 1 | 0.82 | 0.75 | 0.63 | 0.83 | 0.69 | 0.82 | 0.49 | 0.65 | 52, 53 and 62 |

This journal is © The Royal Society of Chemistry 2024

*Energy Environ. Sci.*, 2024, **17**, 2369–2380 | **2373**

produced with a lower share of 28% as a by-product from tin slags and during the extraction of niobium, and zinc only with 10% during the primary production of copper, silver, and gold. The values for copper, tungsten, tin, and iron are below 10%.[57] For the short-term perspective, we updated the previous sector competition index (SCI) calculations with current data on value-added from industry sectors provided in the 2023 Criticality Raw Materials list of the European Commission.[55,58] Tantalum has the highest SCI value of 57 points, and vanadium has the lowest SCI value of 13 points. The lack of substitution options is highest for copper, with 70 substitute performance points. Vanadium, iron, and tungsten also have rather high values of 63, 57, and 53 substitute performance points regarding substitute performance. Better substitutes for bismuth, tantalum, zinc, and tin are available, characterized by 46, 41, 38, and 36 substitute performance points.[59]

Market concentration is measured *via* the Herfindahl–Hirschman-index (HHI), which ranges from 0 to 10 000. The concentration is highest for tungsten and bismuth, with an HHI of over 6000, indicating a very high market concentration. Tungsten and bismuth are both mainly produced in China. Vanadium, tantalum, and iron still have a high concentration with values above 1800. The values of tin, zinc, and copper are between 1000 and 1800, indicating a medium concentration in the market. None of the elements has an HHI below 1000, indicating a low market concentration. Concentrations of reserves range between an HHI of 1229 for tin and 4662 for bismuth. Here, again, the values for bismuth; however, they are from 2017 because USGS has discontinued the data series.[52,53]

The political risk is determined by the evaluation of the producing countries (in the present scenario) and the countries with reserves (in the future scenario) by the three categories of political instability, regulation risk (PPI), which shows the mining-friendliness of a country's administration and governance, and regulation risk (HDI), indicating the possibility of stronger regulation due to not-in-my-backyard politics. The evaluation of producing countries regarding the World Governance Indicator "Political Stability and Absence of Violence/Terrorism" results in political instability values between 0.0 and −1.0. The high production shares of tantalum in the

Democratic Republic of Congo, Nigeria, and Brazil and the high production shares of tin in China and Myanmar, combined with low WGI-PV values for those countries, are of concern. Regarding the policy perception index, all elements have values ranging from 27 to 52. The lowest policy perception values are obtained for tantalum, tin, and bismuth. The human development index values are between 0.6 and 0.8 for most elements. Only tantalum has a lower HDI value of 0.58, indicating a low average human development and, hence, a lower risk for additional regulation.

## Supply risk on the elemental level

In the next step, the values of each indicator are normalized to a common scale and weighted. The supply risk (SR) scores all range from 0, which means no contribution to supply risk, to 100, the highest contribution to supply risk. Indicator scores are normalized so that scores of 70 and above represent high risks. The Tables S1–S5 (ESI†) provide additional information on the interpretation and normalization of each indicator. The indicators were weighed so that all four risk groups were equally attributed to the total risk score (25%), and each indicator within a category contributed equally to the group. Therefore, indicators D1 to D4 have the lowest weighting in the present scenario, with 6.25% each, and the concentration indicators in both scenarios each have a weighting of 25%. Normalized values of each indicator are shown for the present scenario in Fig. 2A and the future scenario in Fig. 2B.

The highest average indicator scores of the eight elements in the present scenario are observed for the dependence on primary production (S3, on average 84 points), the production concentration (C3, 73 points), and the scarcity based on reserves (S1, 63 points). In contrast, demand growth from future technology demand (D1, 8 points) and by-product dependence (D2, 28 points) have the lowest average supply risk scores. The spread of the supply risk scores is lowest for the risk emerging from political instability (P1, standard deviation of 6 points, range of 19 points). The scarcity based on reserves (S1) has the highest spread, with a 40-point standard deviation and scores ranging from 0 to 96. The average unweighted score for all indicators and all eight elements is 52 points.
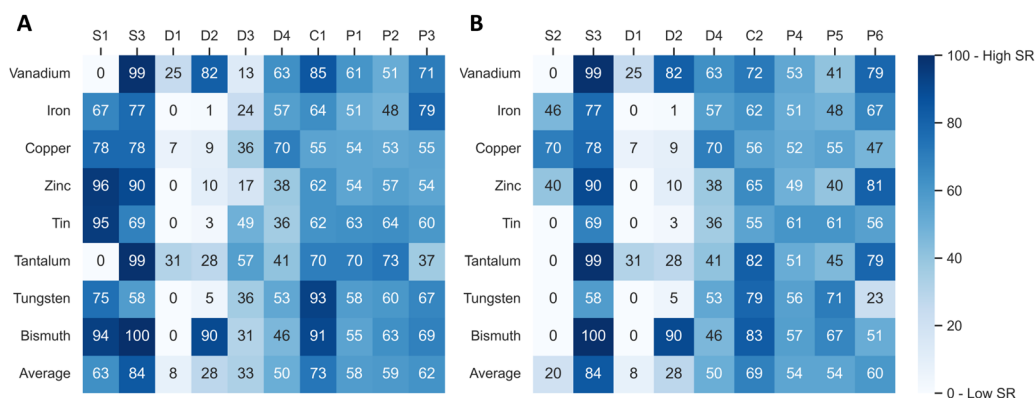


**Present scenario (A)**

| | S1 | S3 | D1 | D2 | D3 | D4 | C1 | P1 | P2 | P3 |
|---|---|---|---|---|---|---|---|---|---|---|
| Vanadium | 0 | 99 | 25 | 82 | 13 | 63 | 85 | 61 | 51 | 71 |
| Iron | 67 | 77 | 0 | 1 | 24 | 57 | 64 | 51 | 48 | 79 |
| Copper | 78 | 78 | 7 | 9 | 36 | 70 | 55 | 54 | 53 | 55 |
| Zinc | 96 | 90 | 0 | 10 | 17 | 38 | 62 | 54 | 57 | 54 |
| Tin | 95 | 69 | 0 | 3 | 49 | 36 | 62 | 63 | 64 | 60 |
| Tantalum | 0 | 99 | 31 | 28 | 57 | 41 | 70 | 70 | 73 | 37 |
| Tungsten | 75 | 58 | 0 | 5 | 36 | 53 | 93 | 58 | 60 | 67 |
| Bismuth | 94 | 100 | 0 | 90 | 31 | 46 | 91 | 55 | 63 | 69 |
| Average | 63 | 84 | 8 | 28 | 33 | 50 | 73 | 58 | 59 | 62 |

**Future scenario (B)**

| | S2 | S3 | D1 | D2 | D4 | C2 | P4 | P5 | P6 |
|---|---|---|---|---|---|---|---|---|---|
| Vanadium | 0 | 99 | 25 | 82 | 63 | 72 | 53 | 41 | 79 |
| Iron | 46 | 77 | 0 | 1 | 57 | 62 | 51 | 48 | 67 |
| Copper | 70 | 78 | 7 | 9 | 70 | 56 | 52 | 55 | 47 |
| Zinc | 40 | 90 | 0 | 10 | 38 | 65 | 49 | 40 | 81 |
| Tin | 0 | 69 | 0 | 3 | 36 | 55 | 61 | 61 | 56 |
| Tantalum | 0 | 99 | 31 | 28 | 41 | 82 | 51 | 45 | 79 |
| Tungsten | 0 | 58 | 0 | 5 | 53 | 79 | 56 | 71 | 23 |
| Bismuth | 0 | 100 | 0 | 90 | 46 | 83 | 57 | 67 | 51 |
| Average | 20 | 84 | 8 | 28 | 50 | 69 | 54 | 54 | 60 |

Colour scale: 100 - High SR (dark) to 0 - Low SR (light)

**Fig. 2** Supply risk values for all indicators of the present scenario (A) and future scenario (B) and all eight elements after normalization.

**2374** | *Energy Environ. Sci.*, 2024, **17**, 2369–2380

This journal is © The Royal Society of Chemistry 2024

The highest average supply risk scores of the eight elements in the future scenario are observed for the dependence on primary production (S3, on average 84 points), the country concentration based on reserves (C2, 69 points), and the regulation (HDI) based on reserves (P6, 60 points). As in the present scenario, demand growth from future technology demand (D1, 8 points) and by-product dependence (D2, 20 points) have the lowest average supply risk scores. The spread of the supply risk scores is lowest for the risk emerging from political instability, based on reserves (P4, standard deviation of 4 points with a range of 12 points). The by-product dependence (D2) has the highest spread, with a 37-point standard deviation and scores ranging from 1 to 90. The average unweighted score for all indicators and all eight elements is 47 points, 5 points lower than in the present scenario.

After the normalization and weighting, aggregating the indicator values for the present scenario gives the relative supply risk score for each of the eight elements, as shown in Fig. 3A. Due to the aggregation and materials typically not being equally critical in all risk categories, element-level supply risk scores have a lower variation than for each indicator. Supply risk scores above 60 should be considered a high risk. The supply risk of bismuth is the highest (73 points), mainly due to the high dependence on primary production, short depletion time, and high market concentration. Iron and copper have the lowest supply risk with 54 points, followed closely by tantalum with 55 points.
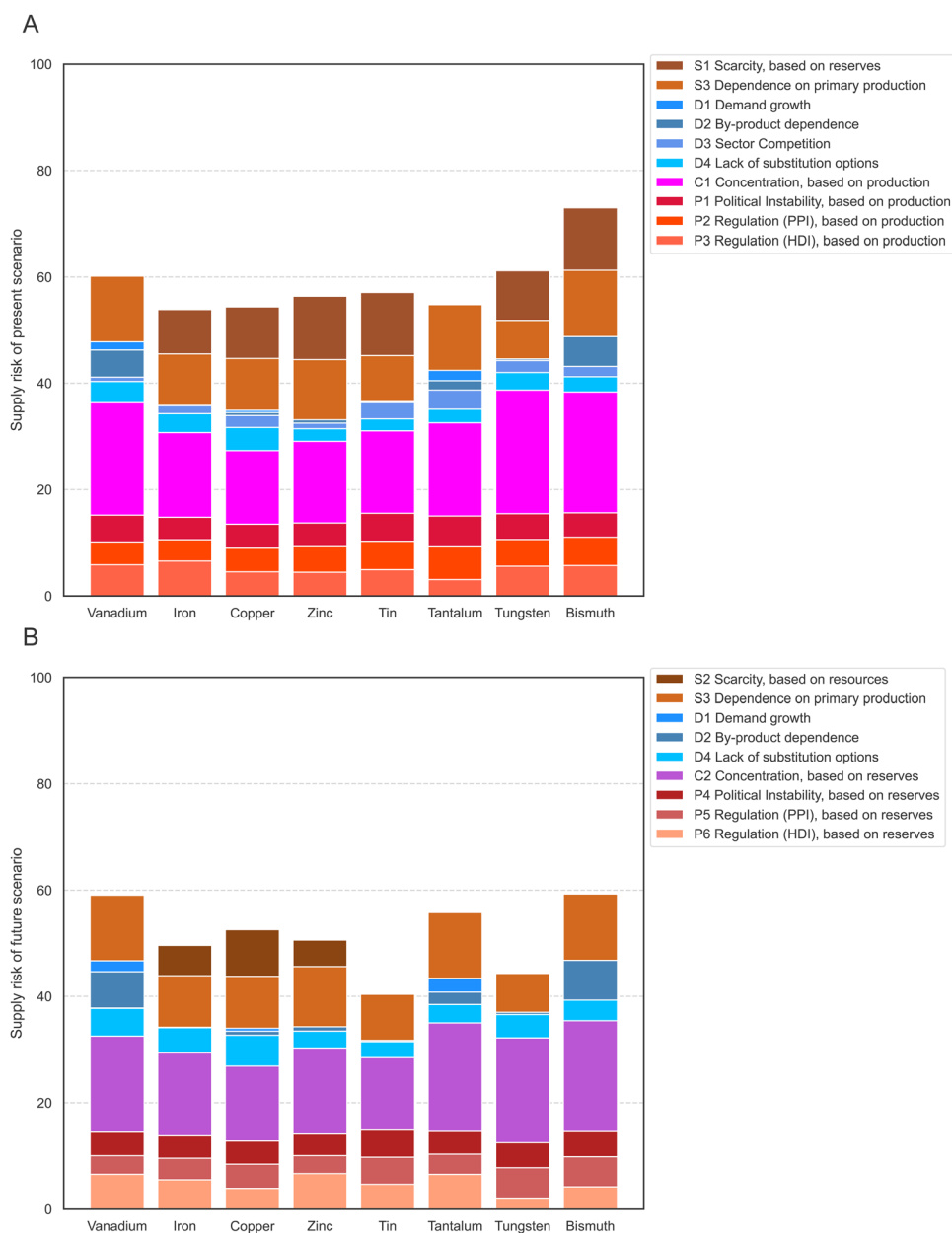


Fig. 3 Supply risk assessment of elements for the present scenario (A) and future scenario (B).

Fig. 3B shows the same elements for the future supply risk scenario. The supply risk of vanadium (59 points) is now only slightly lower than that of bismuth (59 points), while the risk for tantalum stays nearly the same (+1 point). Therefore, vanadium and bismuth have the highest supply risk in the future scenario, mainly due to the omission of the low sector competition risk. The higher weighting of the other demand indicators increases the supply risk values. The vanadium result doesn't change much between the present and the future perspective. However, the former high SR for bismuth significantly drops due to the non-existent scarcity based on resources and a lower concentration risk. The risk for tungsten, which is in the second-highest SR of the elements in the present scenario, is also significantly lower in the future scenario due to the lower scarcity, based on resources, and a lower concentration risk. Tin has the lowest supply risk in the future due to a much lower scarcity. While global tin reserves are limited (4.6 Mt), tin resources are extensive and, if developed, could sustain production well into the future.[52]

Fig. 4 displays the difference in aggregated results of supply risk factors at the element level between the present and future scenarios. The supply reduction indicator group is much higher in the present scenario than in the future. As the indicator dependence on primary production remains the same in both cases, the change of the supply reduction group is due to a change of the indicators S1 and S2, which are scarcity based on reserves and scarcity based on resources. In the future scenario, the values of the indicator scarcity, based on resources, for bismuth, tin, tungsten, tantalum, tin, and vanadium are evaluated with 0 points because the resources are estimated to be sufficient at current production rates for 200 years or longer – in part much longer. The future supply risk score is lower for all elements, except tantalum, with a slight increase from 55 to 56 points. Supply risk scores should, however, be compared between materials within one time perspective, not

primarily between present and future scenario. Lower scores for one element in the future do not mean that the supply risks will ease over time, but rather that supply risks in the long-term are less problematic for this element than they are for other elements.

### Supply risk on the material level

The results on the element level are used to calculate the supply risks on the material level. For this purpose, the scores for each element contained in the absorber materials (see Table 1) are aggregated using the four aggregation methods "equal weighting", "mass-based weighting", "cost-based weighting," and "maximum approach". The ESI† Table S6 explains the calculation and interpretation of all four aggregation methods. The five materials $CuO$, $Cu_2O$, $Ta_3N_5$, $\alpha$-$Fe_2O_4$, and $WO_3$ only contain one supply risk-relevant element; hence, all four aggregation options result in the same supply risk scores, which are also identical to the scores of their supply risk relevant elements shown in Fig. 3. The four materials, $CuBi_2O_4$, $BiVO_4$, $ZnFe_2O_4$, and $\alpha$-$SnWO_4$, contain two evaluated elements each.

The results for the nine absorber materials in all four aggregation methods for the present scenario are shown in Fig. 5A and in the ESI.† In the case of equal weighting, for which each element within the material is weighted equally, $BiVO_4$ results in the highest supply risk with 67 points. The lowest supply risk with 54 points is given for $\alpha$-$Fe_2O_4$, $CuO$, and $Cu_2O$, followed by $Ta_3N_5$ (55 points). Only small changes occur in the mass-based aggregated results. The value of $CuBi_2O_4$ changes from 64 points to 69 points due to the high weight and higher supply risk value of bismuth compared to the lighter and lower-supply risk resulting copper. Changing supply risk results for $BiVO_4$ from 67 points to 70 points are explained by the similar case of heavier, higher-risk bismuth and lighter, lower-risk vanadium. Changes for the supply risk values of $ZnFe_2O_4$ and $\alpha$-$SnWO_4$ are below 1 point. Cost-based
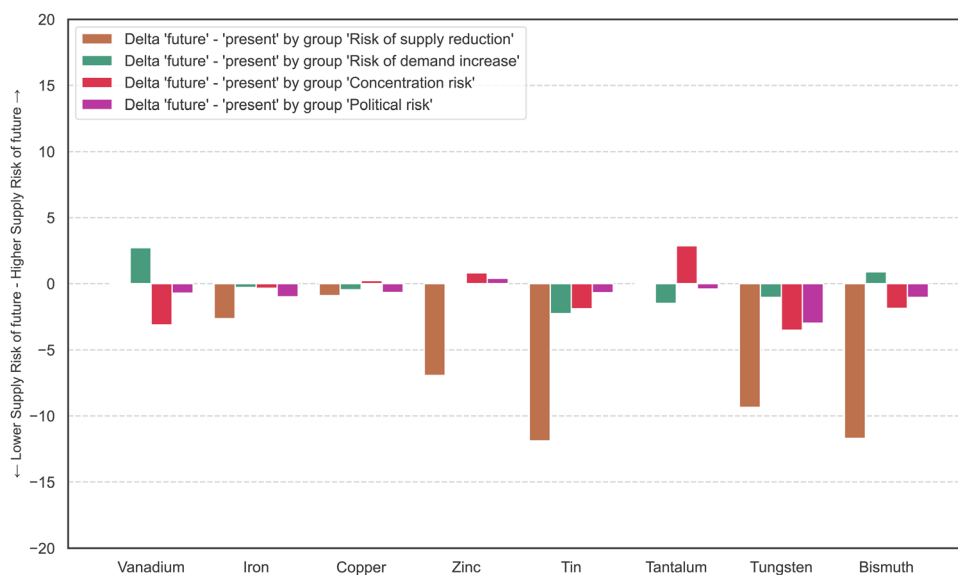


**Fig. 4** Change of the supply risk in each indicator group going from present scenario to future scenario.

aggregation results typically deviate by a maximum of 2 points compared to mass-based aggregated results. The only exception is $BiVO_4$, with 67 points compared to 70 points for mass-based aggregation due to bismuth's higher weight and supply risk, but lower cost. In the maximum approach, values for $CuBi_2O_4$ and $BiVO_4$ are fully determined by the supply risk of bismuth, $ZnFe_2O_4$ results are determined by zinc, and $\alpha$-$SnWO_4$ is determined by tungsten. In summary, $CuBi_2O_4$ and $BiVO_4$ have the highest supply risk values in the present scenario due to the high supply risk of Bi. The lowest supply risk value in the present scenario is obtained for $\alpha$-$Fe_2O_3$ due to the low supply risk of Fe.

In the future scenario, supply risks are slightly lower due to the overall lower risk of supply reduction, as indicated for all elements in Fig. 4. This change also propagates into the supply risk evaluation of absorber materials shown in Fig. 5B and in the ESI.† This applies to all elements and materials with the exception of Ta and $Ta_3N_5$, for which the future risk of supply reduction remains the same, but a higher future concentration risk leads to a higher assessment of the future supply risk. Regarding the equal weighting aggregation, $BiVO_4$ again results in the highest supply risk, this time with 59 points. The lowest supply risk is no longer observed for $\alpha$-$Fe_2O_3$, CuO, and $Cu_2O$ (54 points) but for $\alpha$-$SnWO_4$ with 42 points. Like in the present scenario, changes in the mass-based aggregation compared to equal weighting are only minor. The value of $CuBi_2O_4$ changes from 56 to 58 due to the high weight and higher supply risk value of bismuth compared to the lighter, lower-supply risk copper. Only minor changes of below 1 point are observable for the supply risk values of $BiVO_4$, $ZnFe_2O_4$, and $\alpha$-$SnWO_4$. Cost-

based aggregation results deviate by a maximum of one point compared to mass-based aggregated results for all values, except $\alpha$-$SnWO_4$, with 42 points compared to 40 points in the case of mass-based aggregation due to the higher weight and supply risk of tungsten. General statements regarding maximum aggregation results for the present scenario are also valid for the future scenario. To summarize for the future perspective, $BiVO_4$ still has the highest supply risk values, directly followed by $CuBi_2O_4$, mainly due to the high supply risk of Bi, but also due to the high supply risk value of V. The lowest supply risk value in this case is no longer obtained for $\alpha$-$Fe_2O_3$ but for $\alpha$-$SnWO_4$ due to tin and tungsten's low supply risk values.

## Discussion and conclusion

$BiVO_4$ has been considered for a long time as a benchmark material for photoelectrochemical water oxidation, although its band gap and band positions are not ideal. Many research groups worldwide investigated $BiVO_4$ photoanode optimizations in the last decade. With the right modifications like doping and catalyst decoration, the best photocurrent results for $BiVO_4$ come closest to its theoretical maximum photocurrent compared to other photoanode materials.

Our investigations show that $BiVO_4$ – next to its not-ideal band positions – shows the highest supply risk in seven out of eight combinations of aggregation options (equal, mass, cost, max) within two scenarios (present, future). This is an important finding since $BiVO_4$ is usually considered a non-critical and easy-to-upscale material for large photoanodes.[63] This
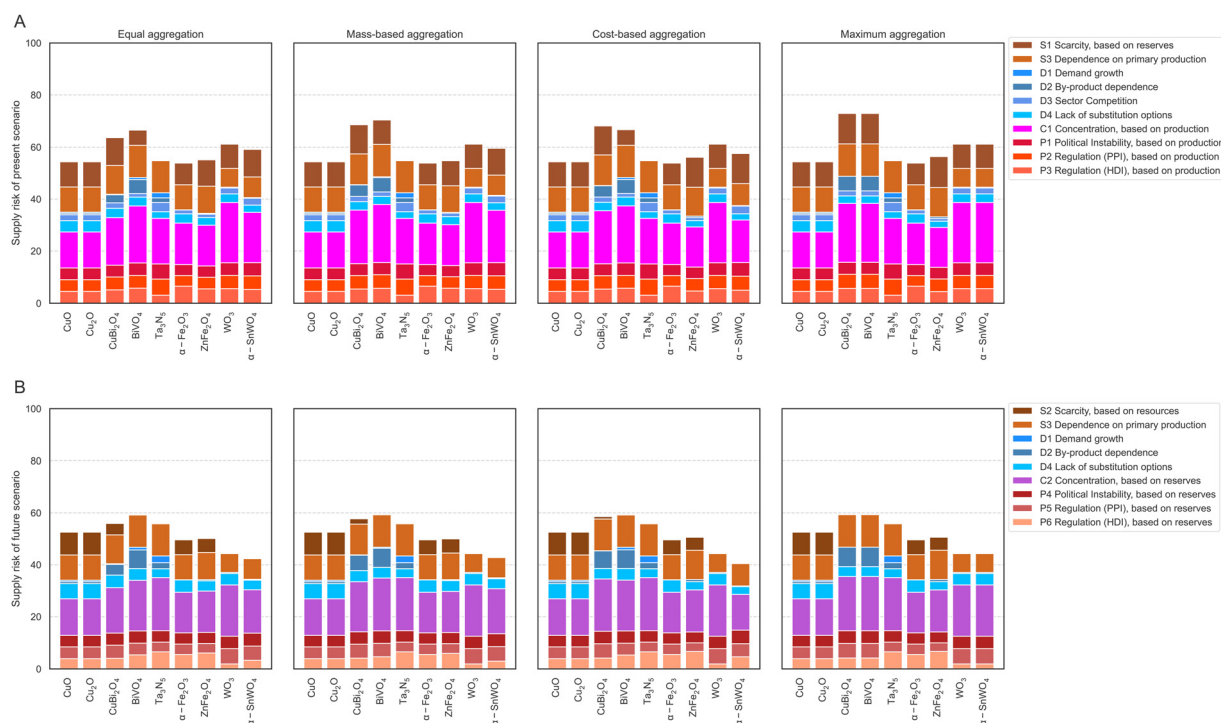


**Fig. 5** Supply risk assessment for present scenario (A) and future scenario (B) using different aggregation methods.

This journal is © The Royal Society of Chemistry 2024

*Energy Environ. Sci.*, 2024, **17**, 2369–2380 | **2377**

upscaling is key for making photoelectrochemical water splitting a substantial contributor to renewable hydrogen production in the future.

On the other hand, $Ta_3N_5$ with a good band gap and good band positions (valence band maximum @1.58 V vs. normal hydrogen electrode (NHE)[64]) can reach 94% of its theoretical photocurrent limit with a multilayer approach,[38] and was recently reported to reach 89% of its maximum possible photocurrent only coated with $FeNiCoO_x$ co-catalyst.[65] In our assessment, $Ta_3N_5$ reaches one of the lowest supply risks within the present scenario, which makes it, in our opinion, a promising photoelectrode materials from a criticality perspective. Moreover, cheap protection layers and catalysts are used to modify $Ta_3N_5$ photoanodes, two points that are not quantitatively considered in our supply risk assessment but make $Ta_3N_5$ photoanodes even more sustainable.

For the iron-based absorbers $\alpha\text{-}Fe_2O_3$ and $ZnFe_2O_4$, supply risk results are equally low in the present scenario as for CuO, $Cu_2O$, and $Ta_3N_5$. For the future scenario, $\alpha\text{-}SnWO_4$ reaches the lowest supply risk directly followed by $WO_3$, which makes tungsten-based options also very promising for future photoelectrode development from a criticality perspective.

Interestingly, the tin supply risk is lower than for iron despite the much larger production quantities in iron mining than in tin mining. Much of the current supply concerns for tin emerge from its low reserve volume compared to annual production, called depletion time. The much higher resource estimation for tin, however, removes concerns about the scarcity of tin from the supply risk evaluation. For iron, this is not equally the case.

Besides many other mixed tungstates, $\alpha\text{-}SnWO_4$ was the first mixed tungstate that achieved reasonable photocurrents exhibiting at the same time suitable band gap for water splitting. Being a self-protecting photoanode material, it was found to need nano-structuring to optimize its performance in the future. Such processing requirements may still limit the large-scale application of otherwise promising photoelectrochemical materials with low supply risk scores.

Our assessments are limited by data availability for the electrochemical properties of promising photoabsorbers. The optimal photocurrents are often only achieved with specific protective materials for each material. This assessment does not include protective layers because of their much lower material demand for the technology. Production processes for applying these thin layers may be very expensive. Furthermore, the comparability of electrochemical properties may be limited due to different measurement procedures in the laboratories of various research groups.

Our assessments are further limited by the data quality for the supply risk assessment. Reserves data for bismuth, for example, was discontinued in 2017 by the USGS. Therefore, this data point is older than all other reserves data we use for the other seven elements. Company concentration data would be an interesting extension of the concentration risk indicator category, but company data was not sufficiently available for the eight elements. Overall, this increases the relative weight of the country concentration of production or reserves on the overall supply risk evaluation. Our assessment focuses on raw material supply risks, not additional supply risks within the supply chain that may occur due to geopolitical trade risks or bottlenecks.

The supply risk assessment could be extended in the future with materials for tandem cells. In those cases, two different materials are combined to achieve a suitable band gap and enable hydrogen and oxygen production despite both materials having unsuitable electrochemical properties. Tandem cells would further increase the amount of possible PEC materials. It is unclear whether this would lead to lower or higher supply risks and is subject to further research.

For criticality assessment researchers, our assessment provides a split of the supply risk assessment into indicators used for the present and future scenarios. Only a few criticality assessments have provided their assessments with specific time horizons, and their indicator selection was always limited. Therefore, we anticipate our analysis will continue the road to a better understanding of the impact of varying time horizons for supply risk and criticality assessments.

## Conflicts of interest

There are no conflicts to declare.

## References

1 S. J. Davis, N. S. Lewis, M. Shaner, S. Aggarwal, D. Arent, I. L. Azevedo, S. M. Benson, T. Bradley, J. Brouwer, Y.-M. Chiang, C. T. M. Clack, A. Cohen, S. Doig, J. Edmonds, P. Fennell, C. B. Field, B. Hannegan, B.-M. Hodge, M. I. Hoffert, E. Ingersoll, P. Jaramillo, K. S. Lackner, K. J. Mach, M. Mastrandrea, J. Ogden, P. F. Peterson, D. L. Sanchez, D. Sperling, J. Stagner, J. E. Trancik, C.-J. Yang and K. Caldeira, *Science*, 2018, **360**, eaas9793.

2 F. Dawood, M. Anda and G. M. Shafiullah, *Int. J. Hydrogen Energy*, 2020, **45**, 3847–3869.

3 S. Wei, R. Sacchi, A. Tukker, S. Suh and B. Steubing, *Energy Environ. Sci.*, 2024, DOI: **10.1039/D3EE03875K.**

4 M. Hermesmann and T. E. Müller, *Prog. Energy Combust. Sci.*, 2022, **90**, 100996.

5 D. Guan, B. Wang, J. Zhang, R. Shi, K. Jiao, L. Li, Y. Wang, B. Xie, Q. Zhang, J. Yu, Y. Zhu, Z. Shao and M. Ni, *Energy Environ. Sci.*, 2023, **16**, 4926–4943.

6 J. Jia, L. C. Seitz, J. D. Benck, Y. Huo, Y. Chen, J. W. D. Ng, T. Bilir, J. S. Harris and T. F. Jaramillo, *Nat. Commun.*, 2016, **7**, 13237.

7 D. Schrijvers, A. Hool, G. A. Blengini, W.-Q. Chen, J. Dewulf, R. Eggert, L. van Ellen, R. Gauss, J. Goddin, K. Habib, C. Hagelüken, A. Hirohata, M. Hofmann-Amtenbrink, J. Kosmol, M. Le Gleuher, M. Grohol, A. Ku, M.-H. Lee, G. Liu, K. Nansai, P. Nuss, D. Peck, A. Reller, G. Sonnemann, L. Tercero, A. Thorenz and P. A. Wäger, *Resour., Conserv. Recycl.*, 2020, **155**, 104617.

**2378** | *Energy Environ. Sci.*, 2024, **17**, 2369–2380

This journal is © The Royal Society of Chemistry 2024

8   T. E. Graedel, E. M. Harper, N. T. Nassar, P. Nuss and B. K. Reck, *Proc. Natl. Acad. Sci. U. S. A.*, 2015, **112**, 4257–4262.

9   P. C. K. Vesborg and T. F. Jaramillo, *RSC Adv.*, 2012, **2**, 7933–7947.

10  T. Hisatomi, J. Kubota and K. Domen, *Chem. Soc. Rev.*, 2014, **43**, 7520–7535.

11  H. Nishiyama, T. Yamada, M. Nakabayashi, Y. Maehara, M. Yamaguchi, Y. Kuromiya, Y. Nagatsuma, H. Tokudome, S. Akiyama, T. Watanabe, R. Narushima, S. Okunaka, N. Shibata, T. Takata, T. Hisatomi and K. Domen, *Nature*, 2021, **598**, 304–307.

12  A. B. Murphy, P. R. F. Barnes, L. K. Randeniya, I. C. Plumb, I. E. Grey, M. D. Horne and J. A. Glasscock, *Int. J. Hydrogen Energy*, 2006, **31**, 1999–2017.

13  M. S. Prévot and K. Sivula, *J. Phys. Chem. C*, 2013, **117**, 17879–17893.

14  Z. Li, W. Luo, M. Zhang, J. Feng and Z. Zou, *Energy Environ. Sci.*, 2013, **6**, 347–370.

15  M. E. Ivanova, R. Peters, M. Müller, S. Haas, M. F. Seidler, G. Mutschke, K. Eckert, P. Röse, S. Calnan, R. Bagacki, R. Schlatmann, C. Grosselindemann, L. Schäfer, N. H. Menzler, A. Weber, R. Van De Krol, F. Liang, F. F. Abdi, S. Brendelberger, N. Neumann, J. Grobbel, M. Roeb, C. Sattler, I. Duran, B. Dietrich, M. E. C. Hofberger, L. Stoppel, N. Uhlenbruck, T. Wetzel, D. Rauner, A. Hecimovic, U. Fantz, N. Kulyk, J. Harting and O. Guillon, *Angew. Chem., Int. Ed.*, 2023, **62**, e202218850.

16  M. R. Shaner, H. A. Atwater, N. S. Lewis and E. W. McFarland, *Energy Environ. Sci.*, 2016, **9**, 2354–2371.

17  C. Helbig, M. Bruckler, A. Thorenz and A. Tuma, *Resources*, 2021, **10**, 79.

18  K. Sivula and R. van de Krol, *Nat. Rev. Mater.*, 2016, **1**, 1–16.

19  A. Kudo and Y. Miseki, *Chem. Soc. Rev.*, 2008, **38**, 253–278.

20  J. Nowotny, T. Bak, M. K. Nowotny and L. R. Sheppard, *Int. J. Hydrogen Energy*, 2007, **32**, 2609–2629.

21  ARTIPHYCTION, https://www.artiphyction.org/, (accessed February 27, 2024).

22  J. H. Kim, D. Hansora, P. Sharma, J.-W. Jang and J. S. Lee, *Chem. Soc. Rev.*, 2019, **48**, 1908–1971.

23  B. A. Pinaud, J. D. Benck, L. C. Seitz, A. J. Forman, Z. Chen, T. G. Deutsch, B. D. James, K. N. Baum, G. N. Baum, S. Ardo, H. Wang, E. Miller and T. F. Jaramillo, *Energy Environ. Sci.*, 2013, **6**, 1983.

24  D. K. Bora, A. Braun and E. C. Constable, *Energy Environ. Sci.*, 2013, **6**, 407–425.

25  J. H. Kim, H. E. Kim, J. H. Kim and J. S. Lee, *J. Mater. Chem. A*, 2020, **8**, 9447–9482.

26  W.-H. Cheng, M. H. Richter, M. M. May, J. Ohlmann, D. Lackner, F. Dimroth, T. Hannappel, H. A. Atwater and H.-J. Lewerenz, *ACS Energy Lett.*, 2018, **3**, 1795–1800.

27  F. F. Abdi, L. Han, A. H. M. Smets, M. Zeman, B. Dam and R. van de Krol, *Nat. Commun.*, 2013, **4**, 2195.

28  D. Bae, B. Seger, P. C. K. Vesborg, O. Hansen and I. Chorkendorff, *Chem. Soc. Rev.*, 2017, **46**, 1933–1954.

29  R. Siavash Moakhar, S. M. Hosseini-Hosseinabad, S. Masudy-Panah, A. Seza, M. Jalali, H. Fallah-Arani, F. Dabir, S. Gholipour, Y. Abdi, M. Bagheri-Hariri, N. Riahi-Noori, Y.-F. Lim, A. Hagfeldt and M. Saliba, *Adv. Mater.*, 2021, **33**, 2007285.

30  S. W. Hwang, G. S. Han, J. Y. Cho, D. U. Lee, H. S. Han and I. S. Cho, *Appl. Surf. Sci.*, 2022, **585**, 152632.

31  J. Li and N. Wu, *Catal. Sci. Technol.*, 2015, **5**, 1360–1384.

32  L. Pan, J. H. Kim, M. T. Mayer, M.-K. Son, A. Ummadisingu, J. S. Lee, A. Hagfeldt, J. Luo and M. Grätzel, *Nat. Catal.*, 2018, **1**, 412–420.

33  C. Li, T. Hisatomi, O. Watanabe, M. Nakabayashi, N. Shibata, K. Domen and J.-J. Delaunay, *Energy Environ. Sci.*, 2015, **8**, 1493–1500.

34  Q. Zhang, B. Zhai, Z. Lin, X. Zhao and P. Diao, *J. Phys. Chem. C*, 2021, **125**, 1890–1901.

35  S. P. Berglund, F. F. Abdi, P. Bogdanoff, A. Chemseddine, D. Friedrich and R. van de Krol, *Chem. Mater.*, 2016, **28**, 4231–4242.

36  F. Wang, W. Septina, A. Chemseddine, F. F. Abdi, D. Friedrich, P. Bogdanoff, R. van de Krol, S. D. Tilley and S. P. Berglund, *J. Am. Chem. Soc.*, 2017, **139**, 15094–15103.

37  Y. Pihosh, I. Turkevych, K. Mawatari, J. Uemura, Y. Kazoe, S. Kosar, K. Makita, T. Sugaya, T. Matsui, D. Fujita, M. Tosa, M. Kondo and T. Kitamori, *Sci. Rep.*, 2015, **5**, 11141.

38  G. Liu, S. Ye, P. Yan, F. Xiong, P. Fu, Z. Wang, Z. Chen, J. Shi and C. Li, *Energy Environ. Sci.*, 2016, **9**, 1327–1334.

39  J.-W. Jang, C. Du, Y. Ye, Y. Lin, X. Yao, J. Thorne, E. Liu, G. McMahon, J. Zhu, A. Javey, J. Guo and D. Wang, *Nat. Commun.*, 2015, **6**, 7447.

40  K.-Y. Yoon, J. Park, M. Jung, S.-G. Ji, H. Lee, J. H. Seo, M.-J. Kwak, S. Il Seok, J. H. Lee and J.-H. Jang, *Nat. Commun.*, 2021, **12**, 4309.

41  Y. Liu, M. Xia, L. Yao, M. Mensi, D. Ren, M. Grätzel, K. Sivula and N. Guijarro, *Adv. Funct. Mater.*, 2021, **31**, 2010081.

42  X. Zhu, N. Guijarro, Y. Liu, P. Schouwink, R. A. Wells, F. Le Formal, S. Sun, C. Gao and K. Sivula, *Adv. Mater.*, 2018, **30**, 1801612.

43  R. A. Henning, P. Uredat, C. Simon, A. Bloesser, P. Cop, M. T. Elm and R. Marschall, *J. Phys. Chem. C*, 2019, **123**, 18240–18247.

44  S. Wang, H. Chen, G. Gao, T. Butburee, M. Lyu, S. Thaweesak, J.-H. Yun, A. Du, G. Liu and L. Wang, *Nano Energy*, 2016, **24**, 94–102.

45  M. Kölbach, I. J. Pereira, K. Harbauer, P. Plate, K. Höflich, S. P. Berglund, D. Friedrich, R. van de Krol and F. F. Abdi, *Chem. Mater.*, 2018, **30**, 8322–8331.

46  W. Qiu, Y. Zhang, G. He, L. Chen, K. Wang, Q. Wang, W. Li, Y. Liu and J. Li, *ACS Appl. Energy Mater.*, 2022, **5**, 11732–11739.

47  G. He, J. Li, W. Qiu, L. Chen, K. Wang, Y. Liu, M. Liu and W. Li, *Chem. Eng. J.*, 2023, **469**, 144096.

48  Y. Xiao, Z. Fan, M. Nakabayashi, Q. Li, L. Zhou, Q. Wang, C. Li, N. Shibata, K. Domen and Y. Li, *Nat. Commun.*, 2022, **13**, 7769.

49  C. Helbig, A. M. Bradshaw, C. Kolotzek, A. Thorenz and A. Tuma, *Appl. Energy*, 2016, **178**, 422–433.

50  C. Helbig, A. M. Bradshaw, L. Wietschel, A. Thorenz and A. Tuma, *J. Cleaner Prod.*, 2018, **172**, 274–286.

51  C. Helbig, A. M. Bradshaw, A. Thorenz and A. Tuma, *Resources*, 2020, **9**, 106.

This journal is © The Royal Society of Chemistry 2024

*Energy Environ. Sci.*, 2024, **17**, 2369–2380 | **2379**

52 USGS, *Mineral commodity summaries 2023*, U.S. Geological Survey, 2023.

53 USGS, *Mineral Commodity Summaries 2017*, U.S. Geological Survey, 2017.

54 T. E. Graedel, J. Allwood, J.-P. Birat, M. Buchert, C. Hagelüken, B. K. Reck, S. F. Sibley and G. Sonnemann, *Recycling rates of metals: a status report, United Nations Environment Programme, and Working Group on the Global Metal Flows*, 2011.

55 European Commission, *Study on the Critical Raw Materials for the EU 2023 Final Report*, Publications Office of the European Union, Luxembourg, 2023.

56 F. Marscheider-Weidemann, S. Langkau, E. Eberling, L. Erdmann, M. Haendel, M. Krail, A. Loibl, C. Neef, M. Neuwirth, L. Rostek, S. Shirinzadeh, D. Stijepic, L. A. Tercero Espinoza, S.-J. Baur, M. Billaud, O. Deubzer, F. Maisel, M. Marwede, J. Rückschloss and M. Tippner, *Rohstoffe für Zukunftstechnologien 2021: "Auftragsstudie,"* Deutsche Rohstoffagentur (DERA) in der Bundesanstalt für Geowissenschaften und Rohstoffe (BGR), Berlin, Datenstand: Mai 2021, Aktualisierung im August 2021., 2021.

57 N. T. Nassar, T. E. Graedel and E. M. Harper, *Sci. Adv.*, 2015, **1**, e1400180.

58 C. Helbig, C. Kolotzek, A. Thorenz, A. Reller, A. Tuma, M. Schafnitzel and S. Krohns, *Sustainable Mater. Technol.*, 2017, **12**, 1–8.

59 T. E. Graedel, E. M. Harper, N. T. Nassar and B. K. Reck, *Proc. Natl. Acad. Sci. U. S. A.*, 2015, **112**, 6295–6300.

60 The World Bank, Worldwide Governance Indicators | DataBank, **https://databank.worldbank.org/source/worldwide-governance-indicators**, (accessed December 11, 2023).

61 J. Yunis and E. Aliakbari, *Fraser Institute Annual Survey of Mining Companies 2021*, Fraser Institute, 2022.

62 UNDP, *Human Development Index*, United Nations Development Programme, 2023.

63 A. Qayum, M. Guo, J. Wei, S. Dong, X. Jiao, D. Chen and T. Wang, *J. Mater. Chem. A*, 2020, **8**, 10989–10997.

64 M. Higashi, K. Domen and R. Abe, *Energy Environ. Sci.*, 2011, **4**, 4138–4147.

65 Y. Pihosh, V. Nandal, R. Shoji, R. Bekarevich, T. Higashi, V. Nicolosi, H. Matsuzaki, K. Seki and K. Domen, *ACS Energy Lett.*, 2023, **8**, 2106–2112.

**2380** | *Energy Environ. Sci.*, 2024, **17**, 2369–2380

This journal is © The Royal Society of Chemistry 2024